A Novel Synthetic Method To Obtain Highly Crystallizable Absorbable Copolyesters

Saša Andjelić,* Dennis D. Jamiolkowski, Brian M. Kelly, and Hugh Newman

Ethicon Products Worldwide, Wound Closure R&D, ETHICON, a Johnson & Johnson Company, Route 22 West, Somerville, New Jersey 08876-0151

Received July 22, 2003; Revised Manuscript Received August 21, 2003

ABSTRACT: A series of undyed 90/10 (mol %) poly(*p*-dioxanone-*co*-glycolide) block copolymers were synthesized by ring-opening polymerization, with stannous octoate as a catalyst, utilizing various ratios of monofunctional initiator, dodecanol (DD), to difunctional initiator, diethylene glycol (DEG). The effect of using combinations of DD and DEG on supramolecular crystalline morphology and crystallization kinetics of prepared polylactone copolymers is examined using calorimetric, optical, and X-ray measurements. We found, unexpectedly, that the absorbable copolymer made with the specific initiator ratio of 50/50 (mol %) exhibits outstanding crystallization properties, crystallizing at radically faster rate and to a higher extent than its counterparts made with either DD or DEG alone. The nucleation density of this material is extremely high compared to those of the other copolymers in the series and is even higher than that of the homopolymer, poly(*p*-dioxanone) (PDS). This unusual behavior is partially explained by the large presence of the longest blocky sequences of glycolate moieties which can serve as effective nucleation sites and strongly facilitate subsequent crystallization of the major PDS phase.

Introduction

Recent advances in the ring-opening polymerization (ROP) of various lactones, such as glycolide or the lactides, have been attributed not only to the development of new classes of organometalic compounds which effectively catalyze these reactions[1−5] but also in a large extent to the growing list of small and high molecular weight species that actually initiate polymerization.[6−14] Regarding catalysts, stannous octoate [tin(II) 2-ethylhexanoate, $Sn(Oct)_2$] has emerged as one of the more effective in ROP capable of producing high yields and high molecular weight. Its reactivity in a bulk polymerization is advantageous: more reactive and the polymerization is difficult to control due to exothermic heat evolution leading to byproduct formation; less reactive and the process is uneconomical with extended reaction times. Stannous octoate is commercially available, shows minimal complexation in solution, and has been used in the preparation of absorbable polymers, from which surgical devices such as sutures have been made and marketed with FDA approval. Two major ROP mechanisms in the presence of $Sn(Oct)_2$ have been proposed: the coordination−insertion mechanism and the activated monomer mechanism. Details of the chemistry of activated species involved in these processes are given elsewhere.[15,16]

To produce a high molecular weight polymer by a ROP in timely and economical fashion, a catalyst such as stannous octoate is usually combined with a mono- or multifunctional initiator. These are mostly hydroxyl-containing compounds, usually primary alcohols, which can be used to generate linear (if the initiator contains one or two alcohol groups) or branched (if three or more groups) polymers. Linear materials utilizing mono- or difunctional initiators, as already alluded to, have found extensive use in producing absorbable surgical devices. Diols have been used in ring-opening "prepolymerizations" to produce α,ω-dihydroxy macroinitiators that are then used in a subsequent copolymerization to produce polymers with special sequence distributions. This sequential addition ROP, in which a monomer feed portion is added in a subsequent step, is one method to make so-called segmented block copolyesters. An example is a glycolide/ϵ-caprolactone copolymer that has enjoyed considerable commercial success.[17]

In the course of the ROP of lactones, it is expected that mono- and difunctional initiators will both normally produce linear materials because one chain, without branch points, is produced from each molecule of initiator. In the absence of transesterification, the molecular weight distributions may be slightly different. (M_w/M_n values of 2 and 1.5 are expected for mono- and difunctional initiated polymerizations, respectively. In the presence of substantial transesterification a value of 2 is approached for both types.) In studying the effect of the functionality of the initiator in the sequential addition ROP of lactones, we explored the use of mono- and difunctional alcohols. We expected the properties of polymers made using a mixture of monofunctional and difunctional initiators to lie between the extremes exhibited by materials based on only monofunctional or only difunctional initiators. In this study, however, we discovered that employing a specific mixture of mono- and difunctional initiators can produce materials with very advantageous properties. They include much more rapid crystallization characteristics with an expected impact in processabilty and mechanical and biological performance enhancements.

Experimental Section

Materials. A series of undyed PDS/Gly block copolymers were prepared by ring-opening polymerization in a metal reactor outfitted with a suitable agitator, as described below, using stannous octoate (Ethicon, Cornelia, GA; total tin 29% w/w) at a monomer-to-catalyst mole ratio of 30 000:1, utilizing various ratios of monofunctional initiator, dodecanol (DD), to a difunctional initiator, diethylene glycol (DEG).

* To whom correspondence should be addressed: e-mail sandjeli@ethus.jnj.com; Tel 908 218 2703; Fax 908 218 3247.

10.1021/ma035052y CCC: $25.00
Published on Web 09/27/2003

Table 1. Properties of a Series of Prepolymers after the First PDS Homopolymerization Stage Prior to Glycolide Charge at 110 °C

polymer	DD/DEG feed molar ratio (%)	*p*-dioxanone conversion (mol %)	M_w (g/mol)	M_n (g/mol)	M_w/M_n	DP_n
1A	100/0	82	51 000	20 000	2.55	196
1B	75/25	85	45 000	22 000	2.05	216
1C	50/50	85	38 000	20 000	1.90	196
1D	25/75	87	52 000	26 000	2.00	256
1E	0/100	84	38 000	23 000	1.65	225

Table 2. Properties of Dried 90/10 PDS/Gly Copolymers Used in This Study

polymer	DD/DEG feed molar ratio (%)	overall monomer-to-initiators ratio	*IV* (dL/g)	M_w (g/mol)	M_n (g/mol)	M_w/M_n
1A	100/0	~1200:1	1.73	80 000	28 000	2.85
1B	75/25	~1000:1	1.77	73 000	27 000	2.70
1C	50/50	~1000:1	1.61	68 000	24 000	2.83
1D	25/75	~1000:1	1.55	55 000	24 000	2.30
1E	0/100	~800:1	1.41	49 000	22 000	2.20

The polymerization process used in preparation of the PDS/Gly block copolymers is a two-stage block copolymerization comprising a first stage homopolymerization using 100% *p*-dioxanone (Noramco, Athens, GA; purity 99%) and a second stage block copolymerization with an added monomer composition of 100 mol % glycolide (Ethicon, Cornelia, GA; purity 99%). After the second stage, unreacted *p*-dioxanone monomer (between 6 and 8%) was removed by a vacuum-drying procedure. The overall final composition of dried samples, as determined by ^{1}H NMR analysis, provides a polymer comprising 90 mol % polymerized *p*-dioxanone and 10 mol % polymerized glycolide. The chemical formulas of the PDS homopolymer and the resulting PDS/Gly copolymer are as follows:

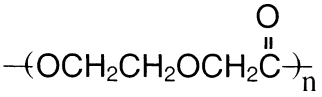

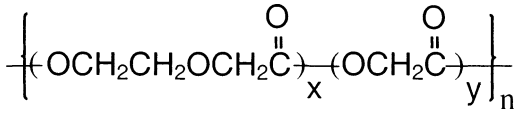

In the first stage of the polymerization, 9 kg of *p*-dioxanone, 9.76 mL of stannous octoate catalyst solution (in toluene, stannous concentration 12% w/v), 9.03 g of DD, and 5.14 g of DEG (DD/DEG ratio for copolymer **1C**) were charged under a nitrogen purge to a clean a dry stainless steel, oil-heated, jacketed reactor equipped with a mechanical agitator. The vessel was evacuated to less than 1 Torr for about 20 min, after which nitrogen gas was introduced to raise the pressure slightly over atmospheric. The evacuation/nitrogen purge process was repeated using a 25 min vacuum-hold period. The constituents were heated under constant agitation to 110 °C and then maintained at this temperature for about $4^1/_2$ h. Selected properties of the prepolymers after the first PDS homopolymerization stage are summarized in Table 1. GPC was used to determine molecular weights of studied materials. The temperature of the oil entering the outer jacket of the reactor was then increased to 135 °C. The second-stage monomer (glycolide, 0.9 kg) was added under nitrogen purge. The stirrer speed was increased to 20 rpm for the first 15 min of the second stage to enhance blending of ingredients. The polymerization was continued for $3^1/_2$ h. The polymer was discharged into trays. After the polymer cooled to room temperature, it was placed into storage bags, weighed, and transferred to freezer storage. The frozen polymer was subsequently ground and sieved—size reduction and classification—and dried under vacuum at elevated temperature. Selected properties of dried polymers are displayed in Table 2. Glycolide monomer is completely consumed in all copolymers, while residual *p*-dioxanone concentration ranges from 0.20 to 0.34 mol % as revealed by ^{1}H NMR. A small difference in molecular weights arises from different concentrations and functionality of initiators. We will show later that the effect of molecular weight on the crystallization properties of the studied materials in the range examined is minimal. Because of the high sensitivity of these polymers to hydrolytic degradation, materials were stored and tested under strict dry nitrogen conditions.

Techniques. *Differential Scanning Calorimetry (DSC).* Calorimetric results were generated on a TA Instruments differential scanning calorimeter, model 2910 MDSC, using dry N_2 as a purge gas.

Crystallization studies were conducted in three ways: (1) after melting, the sample was cooled under a controlled rate; (2) after melting, the sample was quenched below its glass transition temperature and then heated under a controlled rate, and (3) after melting, the sample is rapidly cooled to a temperature of interest and the crystallization measured under these isothermal conditions.

In a typical nonisothermal crystallization run under a constant heating or cooling rate, a sample weighing around 4 mg was first heated to approximately 35−40 °C above its melting temperature and held in the molten state for 5 min to eliminate crystallinity. From this point, a subsequent cooling step was performed at a constant rate, *q*, and the crystallization exotherm recorded. On the other hand, in constant heating rate experiments, the sample was quenched from its amorphous, melted state to below its glass transition temperature, followed by a controlled heating step.

The experiments on the isothermal melt crystallization of PDS/Gly copolymers were carried out as follows: a sample of about 4 mg was first melted and maintained for 5 min at 140 °C (~40 °C above its melting point) to remove any nucleation sites present in a sample. Subsequently, test materials were rapidly cooled (ca. 35 °C/min) to the constant test (crystallization) temperature. The isothermal method assumes that no crystallization occurs before the sample reaches the test temperature. Crystallization behavior was characterized over a wide range of temperatures, between 20 and 80 °C. The isothermal heat flow curve was then integrated to determine the crystallinity as a function of time. The evolution of crystallinity with time can be assessed from the degree of crystallization, α, which is expressed by the ratio

$$\alpha = \frac{\Delta H_t}{\Delta H_\infty} = \frac{\int_0^t \frac{dQ}{dt}\,dt}{\int_0^\infty \frac{dQ}{dt}\,dt} \qquad (1)$$

where dQ/dt is the respective heat flow, ΔH_t is the partial area between the DSC curve and the time axis at time t, and ΔH_∞ is the total area under the peak and corresponds to the overall heat of crystallization. The degree of crystallization, α, is the crystalline volume fraction developed at time t.

It is worth noting that isothermal and nonisothermal runs were made in randomized order to avoid any bias due to possible molecular weight degradation. All temperature runs for a given polymer were performed on a single sample, and the self-consistency of the data engenders confidence that molecular weight loss during testing is not of a concern.

Hot-Stage Optical Microscopy (HSOM). The optical hot-stage experiments were conducted using a Mettler FP90 central processor with a Mettler FP82HT hot stage to control sample conditions. The hot stage, with nitrogen flow, was mounted on a Nikon SMZ-U microscope utilizing linear polarized light. The instrument is equipped with 1× objective, a set of cross-polarizers, and a 1:10 zoom. Images from the microscope were obtained using a Microimage i308 low light integrating video camera. The digital images were captured and analyzed using Image Pro Plus (version 4.0) imaging software.

Growth rate measurements at each temperature were conducted on freshly prepared films to avoid possible degradation problems that might arise with these hydrolytically unstable polyesters. A small amount of ground polymer was placed on the microscope glass slide and a thin cover glass positioned on top of it. The resulting sandwich was then inserted into a hot-stage block regulated at 140 °C. The polymeric sample was then melted for 5 min under a nitrogen purge. A thin film was obtained by applying a slight pressure on the top of cover glass. Monitoring with a digital micrometer, the polymer thickness was adjusted to 0.135 mm for each sample run. In this study, the samples were melted for 5 min at 140 °C in a separate hot-stage apparatus as described above; they were then quickly brought to a second, already preheated measuring device to perform isothermal measurements.

Wide-Angle X-ray Diffraction (WAXD). Some supporting evidence was obtained by conventional X-ray analysis. The WAXD measurements of the isothermally grown films were carried out on a SiemensHi-Star unit using Cu Kα radiation at the wavelength of 1.542 Å. The instrument was operated at 40 kV and 40 mA with the collimator size of diameter 0.5 mm. The convolution of the X-ray images and the calculation of crystallinity content were conducted using the DIFFRAC PLUS software developed by Siemens.

Results

Investigation of the crystalline morphology and crystallization kinetics of the studied PDS/Gly copolymers was carried out experimentally using hot-stage optical microscopy (HSOM) and differential scanning calorimetry (DSC). These two complementary techniques provide information about the crystallization process: the development of spherulites, in terms of both nucleation and growth which can be accurately described by optical measurements, whereas calorimetric data more precisely reflect the overall rate of crystallization. One of the big advantages of HSOM is that nucleation rates and spherulitic growth rates of the 90/10 PDS/Gly block copolymers can be determined separately,[18] deconvoluting the crystallization process into the two parts. This significantly enhances our understanding of crystallization behavior of these materials.

Spherulitic Crystalline Morphology. A series of optical micrographs were captured during isothermal crystallization of studied copolymers as a function of time. Within the microscope's field, the spherulites display regular Maltese cross shapes; those that nucleated at the same time were roughly the same size at any given time, indicating similar growth rates. Although we found that a single type of crystal characterized each isothermal run, the overall number and growth rates of the resulting crystal structures strongly depended on the degree of undercooling.

Crystallization kinetics during spherulite growth are usually expressed via radius or diameter growth rates,

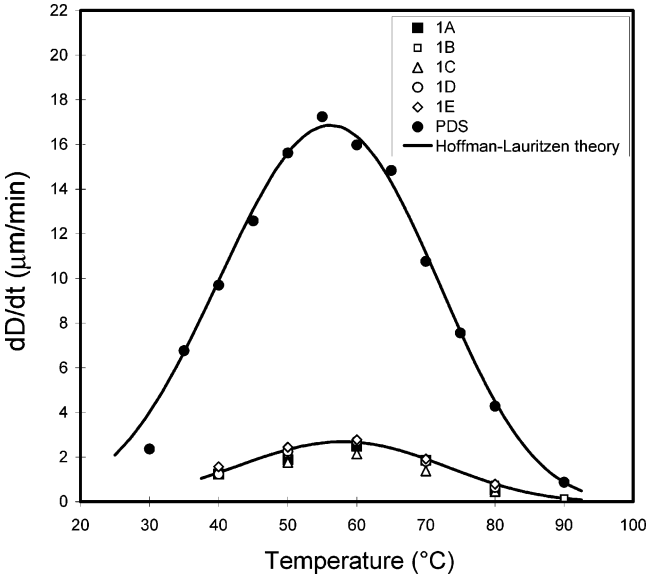

Figure 1. Experimentally obtained spherulitic growth rates, dD/dt (μm/min), obtained at various isothermal crystallization temperatures for copolymers **1A**−**1E** and PDS homopolymer and the expected relationship based on the Hoffman−Lauritzen theory.

dR/dt (dD/dt), where t is the time and R (D) the radius (diameter) of the spherulite, measured by means of an optical micrometer. The general expression of crystal growth is described by Lauritzen and Hoffman[19] as

$$G = \frac{\mathrm{d}R}{\mathrm{d}t} = G_0 \exp\left(-\frac{U^*}{R_0(T_C - T_\infty)}\right) \exp\left(-\frac{K_g}{T_C \Delta T f}\right) \quad (2)$$

where G is the growth rate dR/dt, G_0 is the growth rate constant, U^* represents the activation energy for polymer diffusion, R_0 is the gas constant, and T_C is the crystallization temperature. T_∞ is the temperature at which molecular motion is frozen and viscosity approaches an infinitive value. Hoffman et al.[19] suggest using a value for U^* of 1500 cal/mol and that T_∞ can be approximated by $T_g - 30$, where T_g is the glass transition temperature of the polymer ($T_g = -7$ °C, experimentally found for all our copolymers). The term ΔT in eq 2 stands for the amount of undercooling ($\Delta T = T_m^\circ - T_C$), where T_m° is the equilibrium melting temperature ($T_m^\circ = 140$ °C for the copolymers and PDS, as found by optical microscopy[18]). Parameter f is a dimensionless term expressed by $f = 2T_C/(T_C + T_m^\circ)$. K_g is the nucleation rate constant.

As anticipated, we found that the diameter of the spherulitic formations grew linearly with time over the entire range of investigated crystallization temperatures. The slopes of the curves, dD/dt, systematically increased to a maximum value and then decreased as the melting point was approached. Radial growth ceased only when all surfaces were bounded (impinged). Experimentally determined growth rates, G = dD/dt, are plotted against temperature in Figure 1 for the series of PDS/Gly copolymers and the PDS homopolymer as a comparison. Results showed a characteristic "bell-shaped" dependence between crystal growth rate and crystallization temperature with the maximum rate observed at intermediate temperature zones (58 °C).

The data clearly indicate that for any given crystallization temperature the spherulitic growth rate of PDS homopolymer is significantly higher (~8 times) than

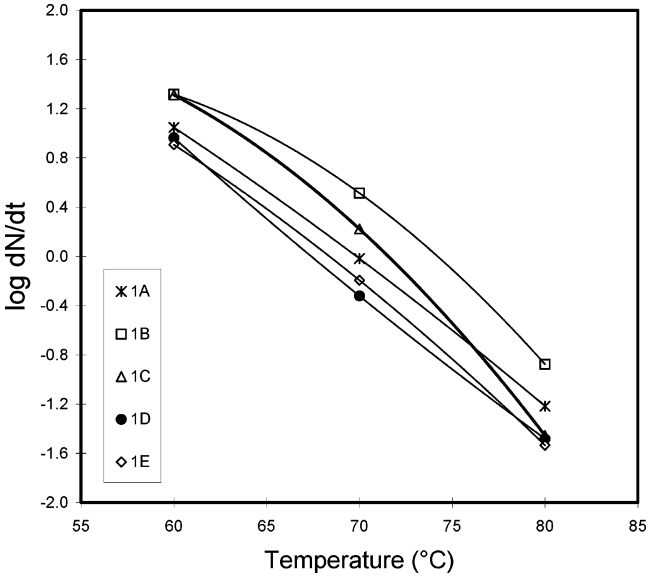

Figure 2. Semilogarithmic plot of nucleation rates (d*N*/d*t*) vs crystallization temperature for copolymers **1A**−**1E**.

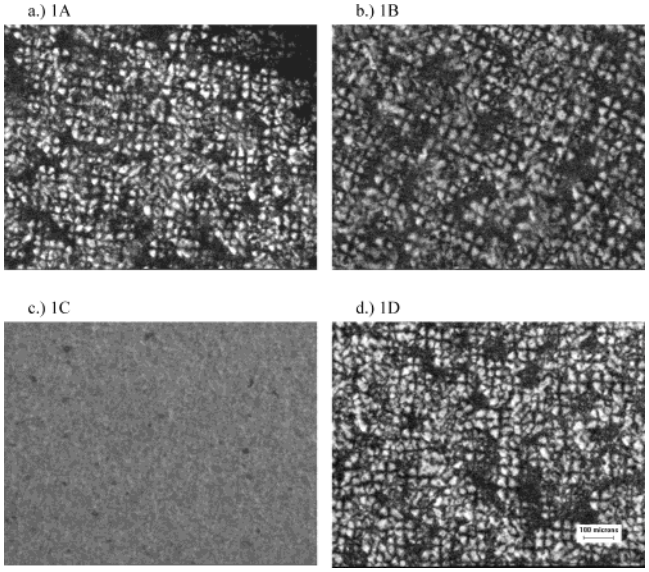

Figure 3. HSOM images of four copolymers captured after 60 min of isothermal crystallization at 40 °C.

those of the copolymer series. The reason for this behavior can be found a disruptive role that comonomer plays in the overall ability of the copolymer's macromolecular chains to align properly for the crystal formation. Also, we noticed that all copolymers in Figure 1 exhibit practically the same spherulitic growth rates regardless of the temperature range used. Solid lines that connect PDS and copolymer **1B** data points were calculated according to eq 2. The excellent fit of the model over a very broad range of temperatures is clearly observed; note that no adjustable parameters are involved in the calculation.

The nucleation density of studied materials was evaluated next. Nucleation density, the number of nuclei per unit volume, generally increases with increasing molecular weight but decreases with increasing crystallization temperature. An estimation of the nucleation rate using hot-stage optical microscopy usually requires a manual counting of nucleation sites present in an arbitrary chosen field of the sample as a function of time. To determine nucleation rates, the initial slopes of these curves (covering the linear region that follows 1−3 min long an induction period) were determined as a function of isothermal crystallization temperatures. Such obtained nucleation rates, d*N*/d*t*, are plotted against temperature for the studied copolymers in a semilog scale in Figure 2. These data suggest that, within the experimentally accessible high-temperature region (60−80 °C), the copolymer **1B** formulation exhibits slightly higher nucleation rates.

The critical data for this study are obtained at temperatures below 60 °C. However, in this experimental range the number of nucleation sites for all studied systems is rather high, preventing the accurate data evaluation. Despite these measurement limitations, we discovered outstanding crystallization properties for the copolymer **1C** formulation at lower crystallization temperatures. Interestingly, the nucleation rates for this specific copolymer observed at higher temperature zone (see the bold line trend of the in Figure 2) were somewhat slower than for copolymer **1B**, but they increased rather abruptly when the crystallization temperature is lowered. The optical images of the copolymer **1C** indicate that due to extensive nucleation, total crystal impingement occurred almost instantaneously. As an illustration, this profound effect was presented in Figure 3, featuring a series of HSOM micrographs of PDS/Gly copolymers captured during isothermal crystallization at 40 °C after 60 min. We found that the nucleation density of copolymer **1C** was extremely high compared to those of the rest of studied copolymers (including copolymer **1E**, data not shown here). Such high nucleation rate dominated the crystallization process even at very early stages. The boundaries of developed structures approached abruptly each other, preventing further spherulite growth. This produced, in turn, a large number of crystals of very small size. We estimate that the average diameter of the copolymer **1C** crystals at the end of crystallization (isothermal run at 40 °C after 60 min) is about 8 μm. The rest of copolymers under the same conditions have a corresponding value significantly higher, about 70 μm.

Overall Crystallization Kinetics by DSC. The overall crystallization rates depend heavily on two factors: the concentration of growing spherulites with time (nucleation dependent) and the rate of spherulitic growth. Contributions of both processes to the overall crystallization kinetics can be studied calorimetrically utilizing controlled isothermal and nonisothermal conditions.

Nonisothermal DSC data generated on the PDS/Gly copolymer series during cooling from the melt show complete agreement with optical measurements. Both methods indicate rapid crystallization of copolymer **1C**. This dramatic effect is illustrated in Figure 4, where a set of thermograms captured during the constant cooling rate (0.5 °C/min) runs is presented for a series of copolymers. Under given experimental conditions, copolymer **1C** produced a large exotherm, suggesting that a significant crystallization took place, while the rest of copolymers barely show any change in the heat flow signal. To characterize the crystallization process, several useful parameters can be extracted from the exotherms shown in Figure 4. The high-temperature slope of the peak may be used to express the crystallization rate under given conditions. The area under the peak is proportional to overall crystallinity in the material. The temperature at the maximum peak

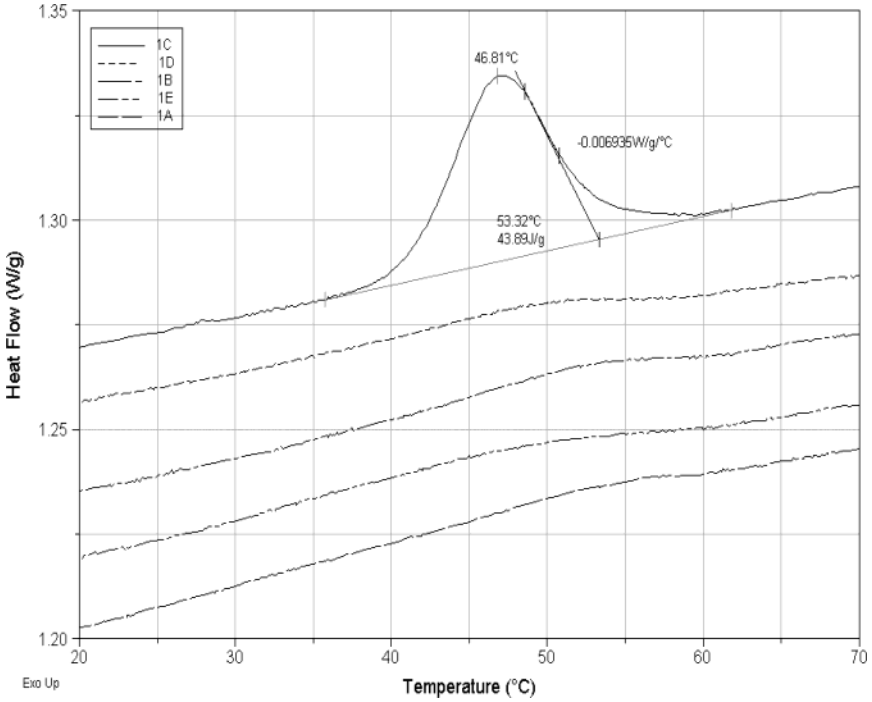

Figure 4. Nonisothermal DSC traces of studied copolymers obtained during crystallization from the melt at a constant cooling rate of 0.5 °C/min. For highly crystallized copolymer **1C** a slope value, heat of crystallization, and crystallization temperatures are also included.

Table 3. Nonisothermal Crystallization Data Obtained during the Constant Cooling Rate of 0.5 °C/min for a Series of Copolymers and a PDS Homopolymer

polymer	T_C (°C)	peak area at T_C (J/g)	α (%)[a]	absolute value of slope[b] (W g^{-1} $°C^{-1}$)	relative rate[c]
copolymer **1A**	52.5	8.2	6.7	0.000 265	0.9×
copolymer 1**B**	52.1	8.9	7.2	0.000 219	0.8×
copolymer **1C**	46.8	43.9	35.3	0.006 940	24.7×
copolymer **1D**	48.5	9.3	7.5	0.000 154	0.5×
copolymer **1E**	48.7	10.2	8.2	0.000 298	1.1×
PDS homopolymer	57.8	39.3	31.7	0.003 810	13.5×

[a] A measure of the crystallinity level, based on a heat of fusion value for 100% crystalline material of 124 J/g. [b] Related to the rate of crystallization. [c] Rate relative to the average of the rate observed for copolymer made with pure monofunctional initiator and for copolymer made with pure difunctional initiator.

Table 4. Nonisothermal Crystallization Data Obtained during Various Constant Cooling Rates for the Copolymer 1C and PDS Homopolymer

polymer	cooling rate (°C/min)	T_C (°C)	peak area at T_C (J/g)	α (%)[a]	slope value (W g^{-1} $°C^{-1}$)
1C	0.25	53.0	43.4	35.0	−0.006 13
	0.50	46.8	43.8	35.3	−0.006 80
	0.75	37.5	33.3	26.9	−0.001 79
	1.00	37.0	25.1	20.2	−0.001 73
PDS homopolymer	0.25	64.0	41.2	33.2	−0.004 16
	0.50	57.8	39.3	31.7	−0.003 81
	0.75	52.3	35.1	28.3	−0.003 75
	1.00	48.4	32.8	26.5	−0.003 67

[a] Based on the heat of fusion for 100% crystalline material = 124 J/g.

indicates the location of the crystallization processes at the given cooling rate. A summary of thermal characteristics for all the copolymers shown in Figure 4 and a PDS homopolymer obtained by the same method is listed in Table 3.

For this set of conditions, copolymer **1C** crystallized radically faster, e.g. 25 times, and to a much higher extent, e.g. 4−5 times, than that of the other copolymers. In addition, about a 2−6 °C lower crystallization temperature observed for polymer **1C** suggests that, in this particular case, the extensive nucleation at lower temperatures is the most dominant crystallization mechanism. Most interestingly, we discovered that both the degree of crystallinity and crystallizability of this material are even higher than those calculated for the PDS homopolymer alone. To further illustrate this behavior, we compared in Table 4 crystallization data between copolymer **1C** and PDS homopolymer obtained using a wide range of DSC cooling rates. At a cooling rate 0.5 °C/min or less, the same trend is observed: copolymer **1C** showed faster crystallization and a higher overall crystallinity than the PDS homopolymer and the balance of the copolymers. This behavior is related to the fact that, for slower cooling cycles, the polymer remains for a longer time at a temperature range sufficiently low for the polymer to begin to crystallize

Table 5. Nonisothermal Crystallization Data Obtained during a Series of Constant Heating Rates for the Copolymer 1C and PDS Homopolymer

polymer	heating rate (°C/min)	T_C (°C)	peak area at T_C (J/g)	α (%)[a]	T_m (°C)
1C	2.5	43.7	43.2	34.8	98.4
	5.0	52.0	43.3	34.9	98.0
	7.5	59.9	40.3	32.5	97.4
	10.0	63.0	26.0	21.0	97.0
PDS	2.0	35.1	34.2	27.6	106.3
homopolymer	4.0	42.4	35.5	28.6	106.0
	8.0	51.7	35.6	28.6	105.5
	15.0	59.4	35.9	28.9	105.3

[a] Based on the heat of fusion for 100% crystalline material = 124 J/g.

but also high enough to provide sufficient chain mobility to facilitate crystal growth. However, by cooling the copolymer sample at rates faster than 0.5 °C/min, we obtained a partially supercooled material, freezing the molecular motion quickly before the chains were able to generate ordered crystals. The result is slower crystallization rates and lower crystallinity content generated for the copolymer at faster cooling steps. This "delay in response" can be explained by the extensive nucleation which dominates the crystallization mechanism of the copolymer **1C** at notably lower temperatures. On the other hand, moderate nucleation and fast crystal growth of PDS homopolymer were initiated at earlier stages of the nonisothermal cooling process, making the crystallization less affected by the higher cooling rates. Under conditions described above, the rest of copolymers in the series crystallize extremely slowly and their parameters cannot be evaluated accurately by the calorimetric methods.

Calorimetric data obtained on PDS/Gly copolymers utilizing controlled heating steps were also analyzed. A typical DSC trace generated using this method shows the crystallization exotherm followed by the melting endothermic process. The area under the crystallization peak equals roughly those for a fusion process, suggesting that the heating scan started from a fully amorphous sample. For all copolymers tested, at the constant heating rate of 10 °C/min, the T_g's of the copolymers in semicrystalline and amorphous states are −3 and −7 °C, respectively. At the same heating rate employed, the materials melts at approximately 98 °C (∼8 °C lower than PDS homopolymer). In addition, the melting point locations obtained after the first (annealed) and second (unannealed) heating runs, as well as the heat of fusion generated on the annealed samples, were almost constant for the test conditions used. On the other hand, because of the significantly higher crystallization rate, the melting peak area of copolymer **1C** (unannealed) samples was much larger than in other copolymers. Using the previous approach, a comparison is made in Table 5 between the melting behavior of highly crystallizable copolymer **1C** and that of the PDS homopolymer evaluated during various heating rates. At the given heating rate used, the copolymer **1C** crystallizes to considerably higher extent than the PDS homopolymer. This unusual finding, obtained under nonisothermal heating conditions, is in line with the relative crystallization rates observed earlier for the samples crystallized under nonisothermal controlled cooling rate experiments. Certain exceptions that are observed for the heating rates of 10 °C/min and higher are caused by the lack of sufficient time for the crystallization to occur; these fast heating rates prevented crystals to fully grow and perfect their morphology.

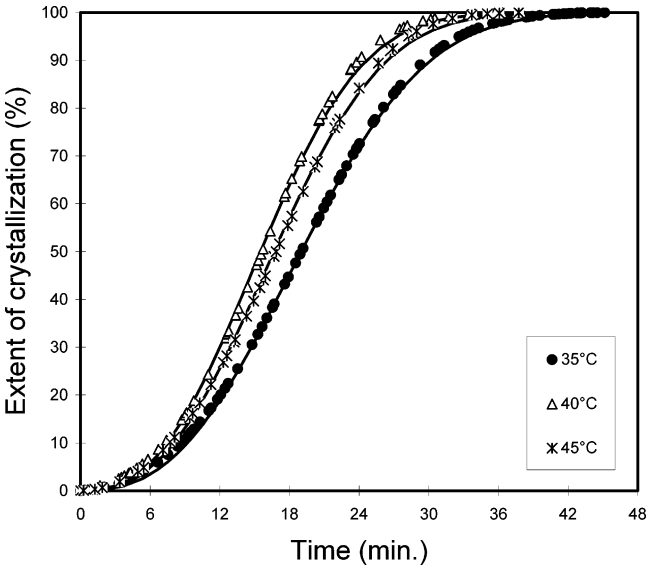

Figure 5. Extent of crystallization (%) as a function of time with annealing temperature as a parameter for the copolymer **1C**. Solid lines are fits to the Avrami equation.

The kinetic data for isothermal melt crystallization of copolymer **1C** were analyzed using a classical Avrami approach. Because of the exceptionally slow crystallization rates observed for the rest of the copolymers during isothermal measurements, their kinetic parameters could not be determined. This reflects the inability of the instrument to account for a continuing incremental crystallization that takes place during these longer-lasting runs. According to the Avrami model, the time dependence of α can be described by the following kinetic expression:

$$-\ln(1-\alpha) = Kt^n \qquad (3)$$

where K is the composite rate constant and n is the Avrami exponent, typically ranging from 2 to 4 for semicrystalline polymers. These constants are related to the crystallization half-time, $t_{1/2}$, and to the type of nucleation and, possibly, the geometry of the crystal growth.

In this study, $t_{1/2}$ was determined by fitting each set of data to eq 3 and then graphically locating the crystallization time that corresponds to $\alpha = 0.5$. Figure 5 displays both experimentally obtained α vs t data and their best fits (solid lines) originated from the Avrami equation for the isothermal crystallization of sample **1C** at selected crystallization temperatures (T_c). As Figure 5 indicates, an excellent fit was observed between the actual data and the theory.

A summary of important kinetic parameters, such as those obtained from Figures 5, is listed in Table 6 for the temperature range between 35 and 60 °C. Data for PDS homopolymer are included in this table as well. The measure of crystallization rates, half-time values, indicates that they are a strong function of T_c. The fastest isothermal crystallization rate (the lowest $t_{1/2}$ value) for the copolymer **1C** was detected at 40 °C. This temperature is lower than that of the homopolymer (45 °C), mainly because of the extensive nucleation mechanism observed for the copolymer at lower temperatures. Despite significantly higher nucleation density, the overall crystallization rates for the copolymer were

Table 6. Isothermal Crystallization Data for the Copolymer 1C and PDS Homopolymer

polymer	T (°C)	$t_{1/2}$ (s)	N	$K(t^{-n})$	ΔH_c (J/g)	α (%)[a]
1C	35	1140	2.60	7.81×10^{-9}	42.1	34.0
	40	930	2.60	1.42×10^{-8}	41.2	33.2
	45	1000	2.59	1.10×10^{-8}	41.1	33.2
	50	1110	2.85	1.49×10^{-9}	44.0	35.5
	60	~2500				
PDS homopolymer	35	570	2.57	5.73×10^{-8}	32.0	25.8
	40	525	2.51	1.03×10^{-7}	31.3	25.2
	45	400	2.41	3.71×10^{-7}	31.2	25.2
	50	470	2.42	2.37×10^{-7}	31.4	25.3
	60	800	2.53	3.24×10^{-8}	39.5	31.8

[a] Based on a heat of fusion value for 100% crystalline material of 124 J/g.

still slower under all studied isothermal conditions. Overall crystallization rates do not exactly follow the nucleation trends observed earlier by HSOM measurements because the second part of the crystallization process for PDS homopolymer—spherulitic growth—is more than 8 times faster at any given temperature (see Figure 1). However, the nucleation effect of copolymer **1C** on the overall isothermal crystallization is still enormous: as indicated in Table 6, the overall crystallization rate for this copolymer is only about half of that for the PDS homopolymer.

The geometry of the crystal habit during isothermal crystallization of the copolymer **1C**, expressed via the Avrami exponent, *n*, is also listed in Table 6. The values of *n* are relatively constant at 2.6, indicating that the crystal structure is three-dimensional and that it was obtained by simultaneous nucleation and crystal growth processes. The slightly lower value was found earlier for the PDS homopolymer (2.5).[20,21] As we mentioned before, the determination of *n* could not be performed on the rest of the copolymer samples using DSC. This was the result of the crystallization rate being so low that the rate of heat gain in the calorimeter was less than the heat-loss rate, resulting in no net change in the enthalpy signal. Finally, the results from Table 6 suggest that crystallization content of copolymer **1C** during the isothermal treatment was significantly higher than for the PDS homopolymer at any given crystallization temperature. This is also in agreement with results obtained during the nonisothermal crystallization measurements utilizing controlled heating and cooling rates. The degree of crystallinity determined from DSC heat of fusion was also confirmed by WAXD.

Discussion

Evidence provided in the previous two sections clearly suggest that the combination of mono- and difunctional initiators added at the specific mole ratio (50/50) during the ring-opening polymerization of 90/10 poly(*p*-dioxanone-*co*-glycolide) produces a material with exceptionally high crystallizability. In addition, we showed that the crystal growth rates of this copolymer stays practically unchanged compared to the rest in the copolymer series, while its nucleation density increases dramatically. In an attempt to further explore this interesting phenomenon, we decided to investigate ^{13}C NMR spectra (UNITYplus, Varian 400 MHz NMR system) of studied copolymers, particularly focusing on sequential distribution of comonomer units. Carbonyl signals in the ^{13}C NMR spectrum of the copolymer **1C** are shown in Figure 6 as an illustration. An assignment of the sequence length distribution has been internally developed at Ethicon for PDS/Gly copolymers based on the original work conducted on the copolymerization of glycolide and ϵ-caprolactone[1] as well as copolymerizations of glycolide and L(−)-lactide and other lactones.[22] The NMR peak integration method of the carbonyl region was conducted on all copolymers, and obtained results relevant to this study are summarized in Table 7. From these calculations we learned that the glycolide portion of copolymer **1C** contains the highest ratio of the longest blocky sequences that may largely contribute to the increased symmetry of the polymer chains (five consecutive Gly repeat units or more in the polymer chain; peak located at 168.9 ppm, column 4 in Table 7) relative to the number of perfectly randomized structures (PDS-Gly-PDS, 169.5 ppm) and various structures that fall in between these two extremes (region from 169.0 to 169.4 ppm). Also, we found that the relative amount of PDS-Gly runs (171.8 ppm, column 3 in Table 7) is the lowest for the copolymer **1C**, further contributing to its predominately "blocky" character. These data indicate that a higher percentage of the longest glycolide blocks in copolymer **1C** may be directly responsible for a large concentration of ordered Gly-containing microdomains (seeds) that can, in turn, rapidly initiate subsequent crystallization of the major PDS phase. The fact that this phenomenon is completely absent in the rest of copolymer series may suggest that some critical concentration of highly ordered Gly sequences (five consecutive Gly repeat units or more) has to exist throughout the polymer matrix, prior to primary crystallization stage, for this particular event to occur.

Our next goal was to investigate the universality of the studied behavior by examining the crystallization properties of different glycolide-containing formulations polymerized by the mixed initiators method. For this purpose, we synthesized two sets of absorbable copolymers: one set having a large overall glycolide content, Gly/ϵ-caprolactone 76/24 (mol %) block copolymer, and the other set, a random copolymer with a much lower Gly content, Gly/L(−)-lactide 5/95. Each of the copolymer sets was prepared using different combinations of mono- and difunctional initiators, as described earlier in the text. Interestingly, in both systems we were able to identify an initiator combination that resulted in a substantial increase in the crystallization rate when compared to data obtained on the other samples in the series. For the Gly/ϵ-caprolactone block copolymer, the optimum ratio was 25/75 (DD to DEG). For the random Gly/L(−)-Lac copolymers, the most rapid crystallization belongs to the sample with the reversed initiator ratio 75/25. However, in contrast to copolymer **1C**, we found that the relative increase in the crystallization kinetics for these two samples was not as profound. For instance, comparing data at the same nonisothermal DSC cooling rate condition (0.5 °C/min), the relative increase of the crystallization rate for both samples is roughly 2−3

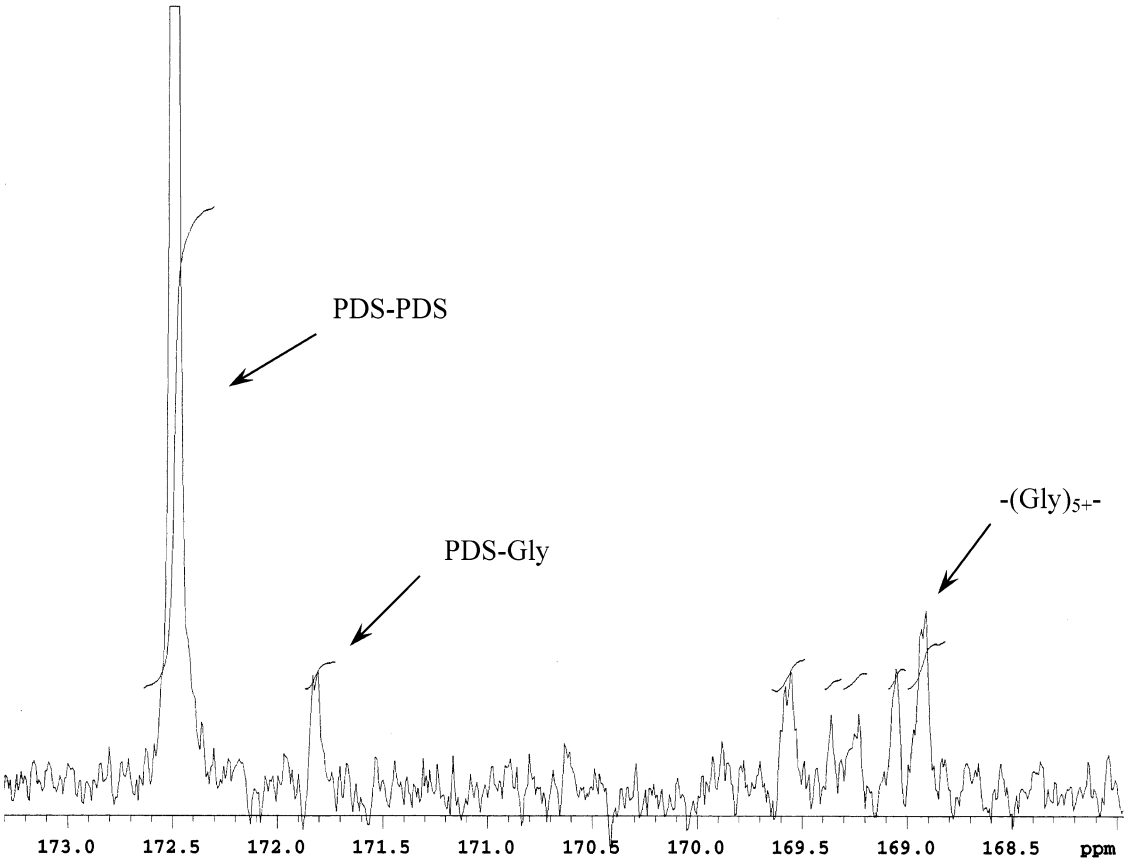

Figure 6. Carbonyl signals in the 400 MHz ^{13}C NMR spectrum of the copolymer **1C** measured in benzene-d_6.

Table 7. Integration of Carbonyl Signals in ^{13}C NMR Spectra of 90/10 PDS/Gly Copolymers Measured in Benzene-d_6 at 30.0 °C[a]

polymer	PDS−PDS [172.5 ppm]	PDS−Gly [171.8 ppm]	-(Gly)$_{5+}$- [168.9 ppm]	PDS in block (%)	Gly in block (%)
1A	1000	56.8	70.4	95.5	36.0
1B	1000	56.6	78.1	94.6	35.2
1C	1000	51.5	104.0	95.1	38.2
1D	1000	64.8	93.0	93.9	34.6
1E	1000	77.5	78.6	92.8	33.9

[a] Acquisition time 1.12 s, observed ^{13}C frequency 100.5 MHz, line broadening 1.0 Hz.

times higher than for those in the rest of a series. This is much less than the impressive 25-fold increase found in the PDS/Gly formulation. In addition, we did not observe any sizable gain in the crystallinity level for the Gly/ϵ-caprolactone or the Gly/L(−)-Lac copolymers. These findings may suggest that the optimal combination of initiators that can be added during ring-opening polymerization of Gly-containing copolymers to enhance the crystallinity performance may be a dual function of glycolide molar participation and the nature and crystallizability of the other constituent in the copolymer.

Conclusion

An absorbable 90/10 (mol %) poly(*p*-dioxanone-*co*-glycolide) block copolymer polymerized using a combination of a monofunctional initiator dodecanol and a difunctional initiator diethylene glycol in a molar ratio of 50/50 exhibited remarkably high crystallizability, compared to the same copolymer prepared using either the mono- or difunctional initiator alone or utilizing any other initiator combination. Crystallization kinetics and overall crystallization content of this formulation studied by both nonisothermal and isothermal conditions increased significantly due to extremely fast nucleation rates observed at lower crystallization temperatures. A superior nucleation rate for this specific copolymer formulation, besides enhancing crystallinity, is likely to produce advantageous small crystal size ideal for manufacturing highly oriented absorbable sutures and small medical implantable devices. This unusually strong nucleation effect was attributed to the presence of favorable blocky sequences in glycolide moieties, which can serve as effective nucleation sites and strongly facilitate subsequent crystallization of the major PDS phase.

Acknowledgment. The authors thank David Orban from the Corporate Product Characterization, Ethicon, for conducting NMR analysis and discussing the results.

References and Notes

(1) Kricheldorf, H. R.; Mang, T.; Jonte, J. M. *Macromolecules* **1984**, *17*, 2173.
(2) Nijenhuis, A. J.; Grijpma, D. W.; Pennings, A. J. *Macromolecules* **1992**, *25*, 6419.
(3) Stevels, W. M.; Ankone, M. J. K.; Dijkstra, P. J.; Feijen, J. *Macromolecules* **1996**, *29*, 3332.
(4) Schwach, G.; Coudane, J.; Engel, R.; Vert, M. *J. Polym. Sci., Polym. Chem. Ed.* **1997**, *35*, 3431.

(5) Xie, W.; Chen, D.; Fan, X.; Li, J.; Wang, P. G.; Cheng, H. N.; Nickol, R. G. *J. Polym. Sci., Polym. Chem.* **1999**, *37*, 3486.
(6) Schindler, A.; Hibionada, Y. M.; Pitt, C. G. *J. Polym. Sci., Polym. Chem. Ed.* **1982**, *20*, 319.
(7) Kricheldorf, H. R.; Lee, S. R. *Macromolecules* **1995**, *28*, 6718.
(8) Trollsas, M.; Hedrick, J. L.; Mecerreyes, D.; Dubois, P.; Jerome, R.; Ihre, H.; Hult, A. *Macromolecules* **1998**, *31*, 2756.
(9) Atthoff, B.; Trollsas, M.; Claesson, H.; Hedrick, J. L. *J. Macromol. Chem., Phys.* **1999**, *200*, 1333.
(10) Joziasse, C. A. P.; Grablowitz, H.; Pennings, A. *J. Macromol. Chem., Phys.* **2000**, *201*, 107.
(11) Tasaka, F.; Ohya, Y.; Ouchi, T. *Macromolecules* **2001**, *34*, 5494.
(12) Wursch, A.; Moller, M.; Glauser, T.; Lim, L. S.; Voytek, S. B.; Hedrick, J. L.; Frank, C. W.; Hilborn, J. G. *Macromolecules* **2001**, *34*, 6601.
(13) Finne, A.; Albertsson, A. C. *Biomacromolecules* **2002**, *3*, 684.
(14) Kricheldorf, H. R.; Fechner, B. *Biomacromolecules* **2002**, *3*, 691.
(15) Kricheldorf, H. R.; Kreiser-Saunders, I.; Boettcher, C. *Polymer* **1995**, *36*, 1253.
(16) Ryner, M.; Stridsberg, K.; Albertsson, A. C.; Schenck, H.; Svensson, M. *Macromolecules* **2001**, *34*, 3877.
(17) Bezwada, R. S.; Jamiolkowski, D. D.; Lee, I. Y.; Agarwal, V.; Persivale, J.; Trenka-Benthin, S.; Erneta, M.; Suryadevara, J.; Yang, A.; Liu, S. *Biomaterials* **1995**, *16*, 1141.
(18) Andjelić, S.; Jamiolkowski, D. D.; McDivitt, J.; Fischer, J.; Zhou, J. *J. Polym. Sci., Polym. Phys. Ed.* **2001**, *39*, 3073.
(19) Hoffman, J. D.; Davis, G. T.; Lauritzen, J. I. In *Treatise on Solid-State Chemistry*; Hannay, N. B., Ed.; Plenum Press: New York, 1976; Chapter 7.
(20) Andjelić, S.; Jamiolkowski, D. D.; McDivitt, J.; Fischer, J.; Zhou, J.; Wang, Z.; Hsiao, B. *J. Polym. Sci., Polym. Phys.* **2001**, *39*, 153.
(21) Andjelić, S.; Fitz, B. D.; Jamiolkowski, D. D. In *Recent Research Developments in Biomaterials*; Ikada, Y., Ed.; Research Signpost: Kerala, India, 2002; Chapter 8.
(22) Kricheldorf, H. R.; Jonte, J. M.; Berl, M. *Makromol. Chem. Suppl.* **1985**, *12*, 25.

MA035052Y